Epithelial cancer detection by oblique-incidence optical spectroscopy

Alejandro Garcia-Uribe, Karthik C. Balareddy, Jun Zou, Kenneth K. Wang, Madeleine Duvic, et al.

Alejandro Garcia-Uribe, Karthik C. Balareddy, Jun Zou, Kenneth K. Wang, Madeleine Duvic, Lihong V. Wang, "Epithelial cancer detection by oblique-incidence optical spectroscopy," Proc. SPIE 7169, Advanced Biomedical and Clinical Diagnostic Systems VII, 71690A (23 February 2009); doi: 10.1117/12.808576

SPIE.

Event: SPIE BiOS, 2009, San Jose, California, United States

Epithelial Cancer Detection by Oblique-Incidence Optical Spectroscopy

Alejandro Garcia-Uribe[1], Karthik C. Balareddy[1], Jun Zou[1], Kenneth K. Wang[2], Madeleine Duvic[3], Lihong V. Wang[4]

[1]Department of Electrical Engineering, Texas A&M University, 3128 TAMU, College Station, Texas, USA
[2]Mayo Clinic, Division of Gastroenterology and Hepatology, Rochester, Minnesota, USA
[3]Department of Dermatology, the University of Texas MD Anderson Cancer Center, 1515 Holcombe Blvd., Houston, Texas, USA
[4]Department of Biomedical Engineering, Washington University in St. Louis, One Brookings Drive, St. Louis, Missouri, USA

ABSTRACT

This paper presents a study on non-invasive detection of two common epithelial cancers (skin and esophagus) based on oblique incidence diffuse reflectance spectroscopy (OIDRS). An OIDRS measurement system, which combines fiber optics and MEMS technologies, was developed. In our pilot studies, a total number of 137 cases have been measured in-vivo for skin cancer detection and a total number of 20 biopsy samples have been measured ex-vivo for esophageal cancer detection. To automatically differentiate the cancerous cases from benign ones, a statistical software classification program was also developed. An overall classification accuracy of 90% and 100% has been achieved for skin and esophageal cancer classification, respectively.

Keywords: oblique incidence, spectroscopy, MEMS, cancer detection.

1. INTRODUCTION

Melanoma is the most serious and a fatal type of skin cancer. The American Cancer Society estimates that there will be 62,000 new cases of melanoma in the U.S. this year with 8,000 people dying of the disease. And there were be about 15,560 new cases of esophageal cancers with about 13,940 deaths in 2007[1]. Esophageal cancer is 3 to 4 times more common among men than among women and 50% more common among African Americans than among whites. Several different optical methodologies have been proposed to determinate the malignancy of tumors[2-4]. Wallace et al.[5] used multivariate discriminate analysis and neural networks to classify reflectance spectra of melanoma and common nevi with an accuracy rate of 86.7%. McIntosh et al.[6] utilized near-infrared reflectance spectroscopy with multivariate analysis to group spectra from non-melanoma skin cancers, pre-cancerous, and benign lesions, with classification accuracies of 72.4-97.7%. Tomatis et al.[7] used multispectral imaging to discriminate between melanoma and non-melanoma lesions with 85% accuracy. Sigurdson et al.[8] employed Raman spectroscopy to categorize skin lesions, including melanoma with a classification performance of 80.5%.

2. EXPERIMENTAL SETUP

The schematic of the system is illustrated in Figure 1. A halogen lamp is used as the light source. The optical multiplexer allows the light delivery through only one source fiber at a time to the area of interest. Once delivered to the skin, the incident light interacts with the medium (skin lesion), whose diffuse reflectance is then collected by the collection fibers. The collection fibers are coupled with the imaging spectrograph (Newport, Oriel MS 257) that generates an optical spectrum for each fiber. The CCD camera (Andor 412DV) collects the spectral-images from the wavelength range of 455 to 765 nm. The spectral images represent the steady-state diffuse reflectance spectra from each collection fiber.

Advanced Biomedical and Clinical Diagnostic Systems VII, edited by Anita Mahadevan-Jansen, Tuan Vo-Dinh, Warren S. Grundfest, Proc. of SPIE Vol. 7169, 71690A

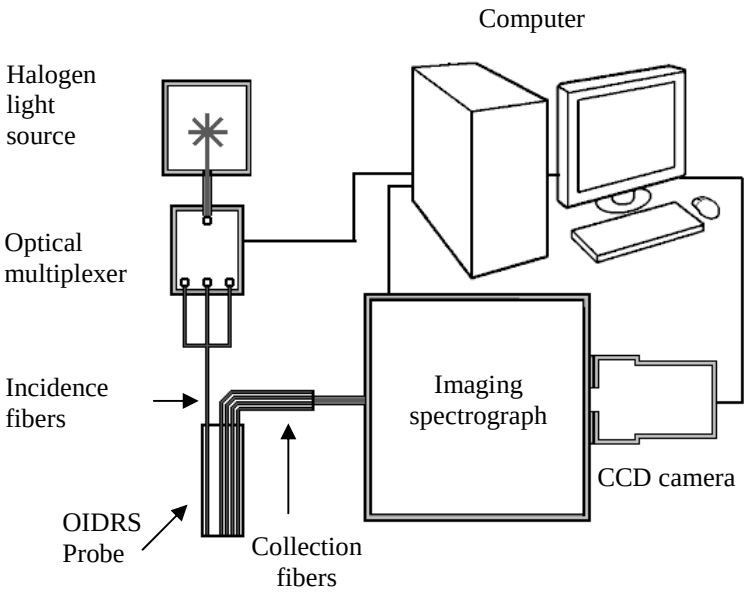

Figure 1: System Setup.

3. PROBE DESIGN AND FABRICATION

The probe for skin was designed with a front view configuration (Fig. 2a). A probe for esophageal cancer needs to be much smaller in size and more importantly side viewing (Fig. 2b). The fiber optic probe for skin lesion consists of five source fibers and 24 collection fibers. The outer casing was made from aluminum as it is easy to machine. The 200 μm plastic-clad silica source fibers are positioned linearly as shown in Fig. 3. When the probe is placed perpendicular to the area of interest, the center source fiber is normal to the surface of incidence. The outer source fibers are situated at 45 degrees and the remaining source fibers were placed at 25 degrees. Two linear arrays, each consisting of twelve silica-silica 100 μm act as collection fibers. The Fig. 4 shows the schematic design of the probe for the ex-vivo esophageal lesion study. An oblique incidence source fiber is used to deliver white light on the tissue surface of interest, which is precisely bent and positioned using a micromachined guide structure. To achieve the "side viewing" capability, a linear array of ten SU-8 waveguides (with a 90^{o} turn) is microfabricated to collect the spatially resolved diffuse reflectance spectra. To minimize light leakage and cross-talk between adjacent collection channels, the SU-8 waveguides are coated with 3000Å of aluminum. Ten interconnection optical fibers are used to interface the SU-8 collection waveguides to the OIDRS measurement system with the assistance of another micromachined guide structure. [9]

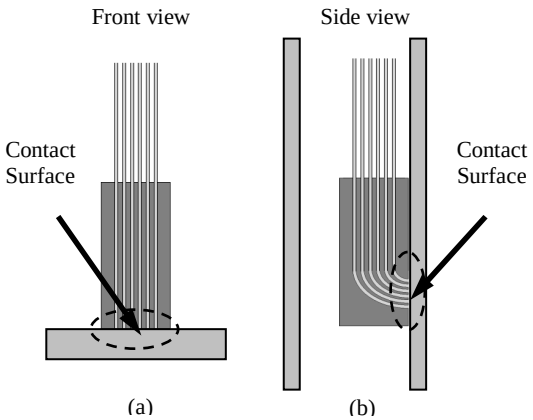

Figure 2. Schematic of OIDRS probe configuration: (a) front viewing and (b) side viewing.

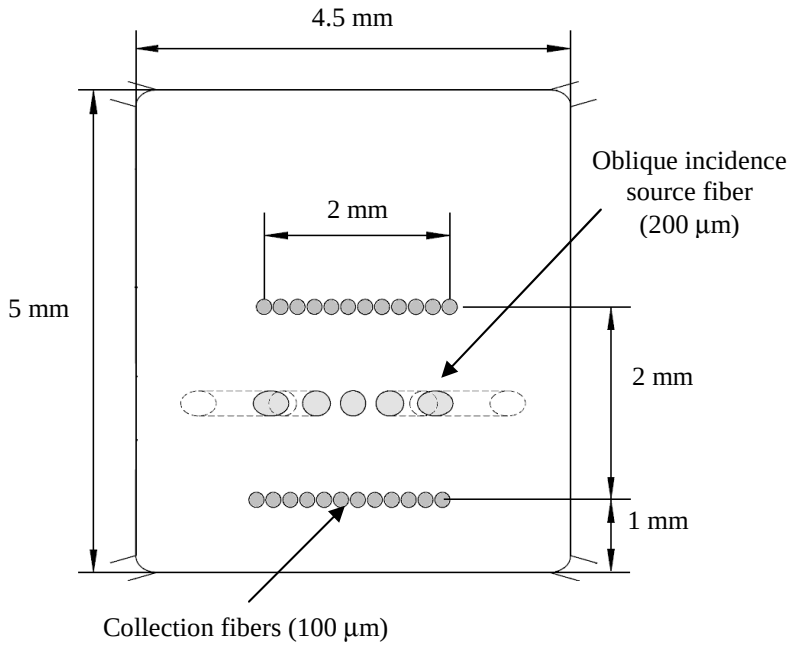

Figure 3. Skin probe description

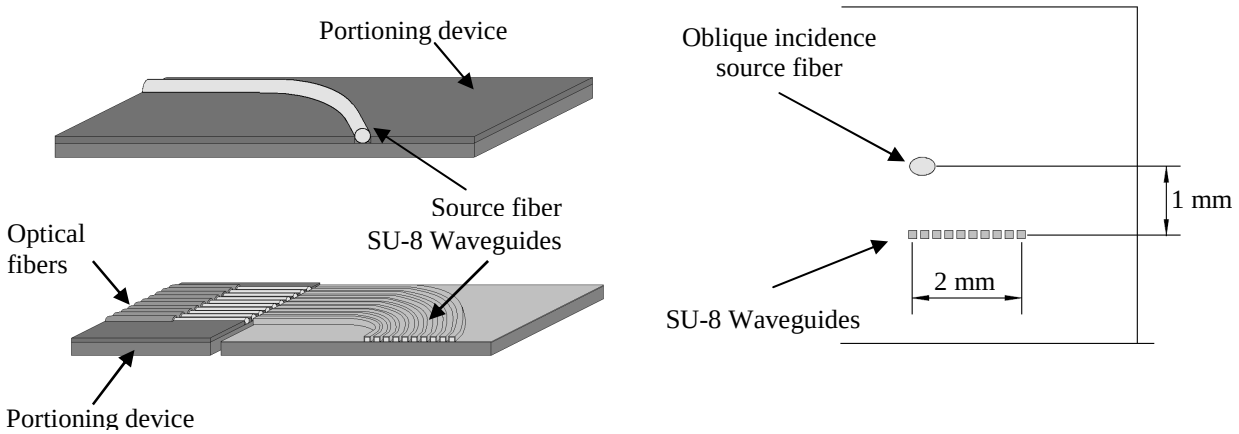

Figure 4. Side view probe description.

4. CLASSIFICATION OF SKIN LESION

Skin data collection was performed at The University of Texas M.D. Anderson Cancer Center (Melanoma and Skin Center). The oblique-incidence spectroscopic probe was used to collect spatio-spectral images from skin lesions and adjacent healthy skin. Data was collected with the probe placed perpendicular to the skin plane, ensuring contact but not compressing the skin. An example of a spectral image is shown in Fig. 5. The spectral images were collected from five source fibers at four probe positions resulting in 20 spatio-spectral images from each lesion and corresponding surrounding healthy tissue. The 137 lesions included in data analysis include common nevi (CN), mildly dysplastic nevi (DN1), moderately dysplastic nevi (DN2), severely dysplastic nevi (DN3), melanoma (M), actinic keratosis (AK), seborrheic keratosis (SK). The data set for skin lesion is described in Table 1.

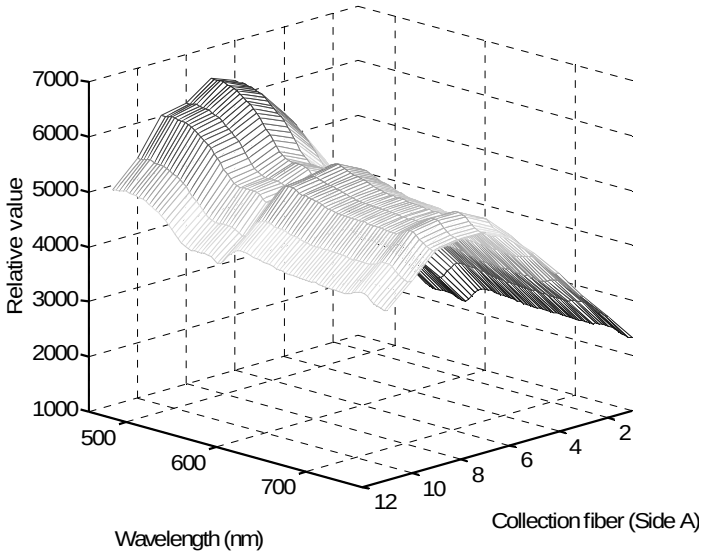

Figure 5. A example of a spatio-spectral data collected from skin.

Each spectral image was normalized by the related healthy tissue image. This is based on the assumption that the melanin content of healthy skin tissue will correlate with that of the imaged lesion. The skin is not homogeneous and will vary within the collection site. To reduce the error, the collection fiber intensity found at each probe position was averaged for each source fiber. Fig. 6 illustrates the classification order followed for pigmented lesions. As describe in ref. 10 the continuous wavelet transform (CWT) was employed to extract the best features per fiber in the two classes under analysis. The most effective features for were chosen using the Fisher distance $FD = |\mu_1 - \mu_2| / \sqrt{\sigma_1^2 + \sigma_2^2}$ as a measure of separability between classes. Where μ_1 and μ_2 denote class means and σ_1 and σ_2 denote class standard deviations. These twenty features form a feature vector that represents each lesion. Before feeding the feature vectors into a classifier the number of feature is optimized using a genetic algorithm. The final feature vectors were processed to remove their correlations and reduce their dimensionality to one dimension. These values are used to design and test a statistical Bayes classifier[11] to separates melanoma from actinic keratosis, seborrheic keratosis, common nevi, and dysplastic nevi. The classification rates for this classifier are 92% for the cancerous lesions and 90% for the benign and dysplastic ones (Table 2).

Table 1. Skin data description.

Common nevi	25
Actinic keratosis	4
Seborrheic keratosis	13
Mild Dysplastic nevi	25
Moderate Dysplastic nevi	51
Severe Dysplastic nevi	6
Melanoma	13
Total	137

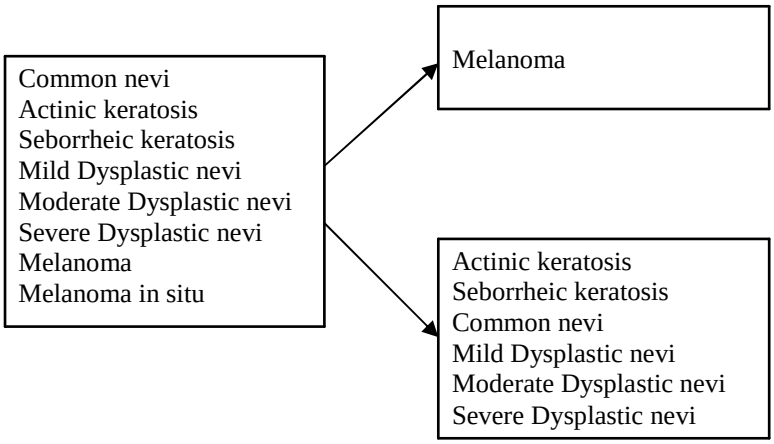

Fig. 6. Breakdown of skin lesions.

Table 2. Classification results for skin lesions.

	Melanoma	DN1, DN2, DN3 CN, AK, SK	Hit rate
Melanoma	12	1	92
DN1, DN2, DN3 CN, AK, SK	13	111	90

5. CLASSIFICATION OF ESOPHAGEAL LESION

The OIDRS system was used to conduct ex-vivo measurement of twenty fresh esophageal samples obtained from patients undergoing endoscopic screening for esophageal diseases at the Barrett's Esophagus Endoscopy Unit of Mayo Clinic (Rochester, MN). The esophageal samples were extracted using endoscopic mucosal resection (EMR) of the esophageal epithelium. The tissue removed averages about 1 cm in diameter with a depth of 0.4 cm. The pathologist can provide information regarding the depth of penetration of the lesion, the size of the lesion, and the margins of resection. After the measurements, the samples were later histopathologically analyzed following the standard procedure at Mayo Clinic. The 20 esophageal samples were found to consist of 8 benign, 6 low dysplastic, 4 highly dysplastic and 2 cancerous lesions (Table 3).

Table 3. Esophageal lesion description.

Benign	6
Low dysplastic	8
High dysplastic	4
Cancerous	2

A bootstrap-based Bayes classifier was designed for esophageal lesion using previously develop algorithm for skin lesion. This classifier separates the benign and low dysplastic from the high dysplastic and cancerous lesion. The classifier generated a classification rate of 100% (100% sensitivity and specificity) (Table 4).

Table 4. Classification results for esophageal lesion.

	Cancerous and high dysplastic	Benign and low dysplastic	Hit rate
Cancerous and high dysplastic	6	0	100
Benign and low dysplastic	0	14	100

6. CONCLUSIONS

This paper presents a study for epithelial cancer detection using oblique-incidence diffuse reflectance spectroscopy. The classifier that distinguishes cutaneous melanoma from benign and dysplastic skin lesions achieves a sensitivity of 92% with a specificity of 90%. The second classifier design to separate esophageal lesions presented a classification rate of 100%. We should notice that the results from the study for classification of ex-vivo esophageal lesions was limited by its small sample size, but these results indicate that the proposed approach can potentially be used by for computer-assisted classification technique of different types of epithelial lesions.

7. ACKNOWLEDGMENT

We thank the staff of the Skin Cancer and Melanoma Center (UTMDACC) and the Division of Gastroenterology and Hepatology (Mayo Clinic) for their help during the data collection. This project is sponsored by NIH grant R01 CA106728.

8. REFERENCES

1. American Cancer Society, Cancer Facts & Figures 2007, Available at http://www.cancer.org.
2. P. R. Bargo, S. A. Prahl, T. T. Goodell, R. A. Sleven, G. Koval, G. Blair, S. L. Jacques, "In vivo determination of optical properties of normal and tumor tissue with white light reflectance and an empirical light transport model during endoscopy," Journal of Biomedical Optics 10, 034018 (2005).
3. S. Brand, J. M. Poneros , B. E. Bouma , G. J. Tearney C. C. Compton , N. S. Nishioka, "Optical Coherence Tomography in the Gastrointestinal Tract," Endoscopy 32, 796-803 (2000)
4. Messmann H, Knüchel R, Bäumler W, Holstege A, Schölmerich J. "Endoscopic fluorescence detection of dysplasia in patients with Barrett's esophagus, ulcerative colitis, or adenomatous polyps after 5-aminolevulinic acid-induced protoporphyrin IX sensitization," Gastrointestinal Endoscopy, 49(1), 97-101 (1999).
5. V. P. Wallace, J. C. Bamber, D. C. Crawford, R. J. Ott, and P. S. Mortimer, "Classification of reflectance spectra from pigmented skin lesions, a comparison of multivariate discriminant analysis and artificial neural networks," Physics in Medicine and Biology 45, 2859-2871 (2000).
6. L. M. McIntosh, R. Summers, M. Jackson, H. H. Mantsch, J. R. Mansfield, M. Howlett, A. N. Crowson, J. W. Toole, "Towards non-invasive screening of skin lesions by near-infrared spectroscopy", Journal of Investigative Dermatology 116 (1), 175-181 (2001).
7. S. Tomatis, M. Carrra, A. Bono, C. Bartoli, M. Lualdi, G. Tragni, A. Colombo, R. Marchesini, "Automated melanoma detection with a novel multispectral imaging system: results of a prospective study", Physics in Medicine and Biology 50, 1675-1687 (2005).
8. S. Sigurdsson, P. A. Philipsen, L. K. Hansen, J. Larsen, M. Gniadecka, and H. C. Wulf, "Detection of Skin Cancer by Classification of Raman Spectra", IEEE Transactions on Biomedical Engineering 51, 1784-1793 (2004).
9. A. Garcia-Uribe, K. C. Balareddy, J. Zou, A. K. Wojcik, K. K. Wang and L. V. Wang, "Micromachined Side-Viewing Optical Sensor Probe for Detection of Esophageal Cancers," Journal of Sensors and Actuators A: Physical, doi:10.1016/j.sna.2008.11.008 (2008).
10. A. Garcia-Uribe, N. Kehtarnavaz, G. Marquez, V. Prieto, M. Duvic, and L. V. Wang, "Skin cancer detection by spectroscopic oblique-incidence reflectometry: classification and physiological origins," Applied Optics 43, 2643-2650 (2004).
11. R. O. Duda, P. E. Hart, and D. G. Stork, Pattern Classification, 2nd ed., New York: Wiley Interscience, (2000).